Ab initio examination of ductility features of fcc metals

Sami Kamran,[1] Kuiying Chen,[2,*] and Liang Chen[1]
[1]*Department of Physics, University of Ottawa, Canada K1N 6N5*
[2]*Institute for Aerospace Research, National Research Council Canada, Canada K1A 0R6*
(Received 29 August 2008; published 12 January 2009)

Through systematic density-functional theory-based *ab initio* calculations, various performance indicators such as G/B, the ratio of shear modulus G over bulk modulus B, σ_s/σ_t, the ratio of ideal shear strength σ_s over tensile strength σ_t, and the Cauchy pressure defined as C_{12}-C_{44} were evaluated for a selection of fcc metals and assessed in relation to the characteristics of their electronic distributions obtained from the electron localization function. The analysis reveals that the ratio σ_s/σ_t is possibly a better indicator of malleability as it discriminates directionally bonded metals in addition to discerning ductile crystals from brittle ones. Furthermore, Al is found to sustain the largest shear deformation among the scrutinized solids due to its directional bonds. Similarly, the surprisingly long range of distortion of Pd is rationalized as a result of the geometric constraints caused by small electron pockets of comparatively high localization in the interionic region. However, the examination of the peculiar case of Ir suggests that, in general, the extent of shear distortion should be the consequence of at least two factors, namely, the angular characteristics of bonding and the bond strength.

DOI: 10.1103/PhysRevB.79.024106 PACS number(s): 61.82.Bg

I. INTRODUCTION

The assessment of the malleability of solids, which is of real significance in engineering and materials science, has motivated a lot of research intended to elaborate various types of criteria allowing the distinction between the ductile and brittle crystals based on experimentally available data. Thus, measurable quantities such as elastic coefficients and surface energy have often been exploited to estimate empirically inaccessible parameters related to the nonlinear behavior of crystals in order to establish different sorts of ratios predicting the ductility of solids in a more or less universal fashion. Rice's ratio of unstable stacking fault energy γ_{us} over surface energy γ_s (γ_{us}/γ_s),[1] Pugh's widely used ratio of shear modulus G over bulk modulus B (G/B),[2] and the Cauchy pressure (C_{12}-C_{44}) (Ref. 3) are examples of broadly known outcomes of such investigations. In the last two decades, the rapidly growing computational materials science has provided the possibility of calculating the ideal strength, defined as the maximal stress sustained by a crystal before failure is attained, and the corresponding strain, recently dubbed shearability (s_m) or tensibility (t_m) depending on the type of distortion withstood by the crystalline structure.[4] These intrinsic properties, which have been approximated by the elastic moduli usually within the context of Franckel's model,[5] permit the direct probe of the response of crystals to deformations of extended scope. Lately, the ideal strengths of bcc tungsten (W) and iron (Fe) have been the subject of detailed study[6,7] while among the fcc metals, copper (Cu) and aluminum (Al) have grabbed the attention of researchers the most due to their wide technological applications.[8] Ogata *et al.*[4] showed that, contrary to the common belief, the shear strength of Al is higher than that of Cu. This feature is attributed to the angular character of Al bonds, which do not allow the bond reformation process to take place once the shear is stopped. This observation gives rise to the suggestion that, in general, directionally bonded solids tend to undergo large ranges of deformation. Nevertheless, our calculations on Ir, which are presented in the current paper, evince that unlike Al, this angularly bonded metal does not suffer a substantial extent of distortion. In view of these different results, there is a compelling need for a systematic analysis of the commonly employed performance indicators such as the G/B ratio, and the information provided by the theoretical strengths and ideally maximal strains with the aim of elucidating the advantages and the drawbacks of each of these malleability measures.

II. CALCULATION METHODOLOGY AND RESULTS

The Vienna *Ab initio* Simulation Package (VASP) (Refs. 9 and 10) based on density-functional theory (DFT) is employed to investigate the behavior of fcc metals under shear and uniaxial tensile deformations. A plane-wave basis set and the Perdew-Wang generalized-gradient approximation (GGA-PW19) (Ref. 11) are used. In the case of Al, the ultrasoft (US) pseudopotential is utilized while for the other fcc crystals (Ag, Cu, Ir, Ni, Pd, and Pt), we opted for the projector-augmented wave (PAW) method.[12,13] The cutoff energies fall within the range of ~440 eV and the convergence of the total-energy calculations were in the order of 10^{-5} eV. In the calculations of the elastic coefficients, the Brillouin-zone integration (BZI) is performed via $17\times17\times17$ Monkhorst-Pack k points while, in the case of shear deformation along the {111} plane and tension simulation for the ⟨111⟩ direction, the BZI is carried out with $17\times17\times9$ k points.

As most frequently utilized ductility measures are either defined or expressible in terms of elastic constants, the first step toward reviewing the aforesaid malleability criteria in connection with the electronic features of chemical bonding consists of computing elastic stiffness coefficients and appropriate moduli, all of which are related to the second derivatives of the total energy. To this end, a conventional four-atom fcc unit cell was constructed and subjected to specific types of deformation for the evaluation of the three indepen-

TABLE I. Lattice parameters, bulk modulus, and the elastic constants of fcc metals. All the values are in GPa except for the lattice constant which is in angstroms. The experimental results are taken from Ref. 15.

Metal		a (Å)	B		C_{11}		C_{12}		C_{44}	
			Calc	Expt	Calc	Expt	Calc	Expt	Calc	Expt
Ag	PAW	4.149 083 5	97.95	99.8	115.8	124	89	93.4	40.7	46.1
Al	US	4.040 191 6	82.2	79	112	108	67.3	62.2	27.2	28.4
Cu	PAW	3.637 416 4	145.4	133.3	176.5	176.4	129.8	129.2	82.3	75.2
Ir	PAW	3.879 316 2	346.9	354.7	582.6	580	229.2	242	258.2	256
Ni	PAW	3.514 247 4	196.1	186.7	252.7	243.6	167.7	149.4	116.3	119.6
Pd	PAW	3.951 166 1	189.5	193.1	220.2	227.1	174.2	176	68.73	71.73
Pt	PAW	3.985 678 2	265.5	282.7	322.4	346.7	237.1	250.7	74.21	76.5

dent elastic coefficients C_{11}, C_{12}, and C_{44}, which characterize the linear stress-strain relation in these crystals. To calculate C_{11}-C_{12}, a tetragonal shear distortion is implemented, whereas the computation of C_{44} is realized through trigonal shear deformation. From the complete set of the elastic coefficients and bulk modulus B, shear modulus G is determined. The details of the calculation of the elastic coefficients and moduli can be found in our previous paper.[14] The calculated elastic constants together with the experimental measurements are displayed in Table I. The accuracy and the reliability of the present computations are demonstrated by the good agreement between the predicted and experimental values.[15] The shear modulus G, the shear modulus $G_{\{111\}}$ along the $\{111\}$ plane, and the Cauchy pressure C' are obtained from the elastic stiffness constants through relations (1)–(3), respectively:

$$G = \tfrac{1}{5}(C_{11} - C_{12} + 3C_{44}), \tag{1}$$

$$G_{\{111\}} = \tfrac{1}{3}(C_{11} - C_{12} + C_{44}), \tag{2}$$

$$2C' = C_{12} - C_{44}. \tag{3}$$

As regards to the theoretical shear and tensile strengths, which portray the large-strain nonlinear response of the material, they are both identified with the maximum values of the gradients of the total-energy density under shear and tensile distortions, respectively. In the current study, the $\{111\}\langle 11\bar{2}\rangle$ slip system is selected to simulate shear processing and the [111] direction is chosen to model tensile deformation. To achieve the aforementioned simulations, a six-atom orthorhombic unit cell whose z axis coincides with the positive [111] direction in the Cartesian coordinate system and of which the y axis is parallel to the [112] vector is used. The modeling of shear distortion requires the rotationlike transformation of the Bravais lattice vectors $\{\vec{a}_i, \vec{b}_i, \vec{c}_i\}$ into the sheared basis $\{\vec{a}_i', \vec{b}_i', \vec{c}_i'\}$ as prescribed below,[16]

$$\vec{a}_i' = S_i^j \vec{a}_j, \tag{4}$$

where

$$S_j^i = \delta_j^i + \gamma b^i n_j. \tag{5}$$

In Eq. (5), δ_j^i is the Kronecker delta, b^i are the contravariant components of a unit vector parallel to the Burgers vector, γ is the dimensionless shear deformation parameter, and n_i corresponds to the covariant components of the normalized slip direction, which is the [111] direction in the case of fcc metallic crystals. It is noteworthy that in Eqs. (4) and (5), the Einstein summation convention is utilized. As for the modeling of tension along the [111] direction, it is realized through extending the length of the unit cell along the z axis of the orthorhombic lattice.

In Table II, the estimations for G, which are used to evaluate Pugh's malleability indicator G/B, and $G_{\{111\}}$ are listed together with our predictions for the ideal shear strength σ_s

TABLE II. The ideal strengths and the corresponding strains together with shear modulus of fcc metals. The theoretical values ($s_{m(\text{theo})}$, $\sigma_{m(\text{theo})}$, and $G_{(111)\text{theo}}$) are taken from Ref. 20 while $s_{m(\text{pres})}$, $\sigma_{m(\text{pres})}$, and $G_{(111)\text{pres}}$ represent the current calculations. Shear moduli and the ideal strengths are in GPa.

Metal	$s_{m(\text{pres})}$	$s_{m(\text{theo})}$	$\sigma_{m(\text{pres})}$	$\sigma_{m(\text{theo})}$	$G_{(111)\text{pres}}$	$G_{(111)\text{theo}}$	t_m	$\boldsymbol{\sigma_t}$
Pd	0.17		2.97		34.04		0.240	21.5
Al	0.20	0.20	3.60	3.73	24.07	25.4	0.253	10
Ir	0.16		20.21		199.76		0.180	47.99
Pt	0.122		2.21		53.04		0.216	25.2
Cu	0.159	0.157	3.48	3.45	45.22	40.9	0.217	20.81
Ni	0.163	0.162	5.02	4.70	63.63	60.5	0.235	32.84
Ag	0.153	0.156	1.88	2.57	23.79	32.2	0.198	11.35

for the $\{111\}\langle 11\bar{2}\rangle$ slip system, the related maximal strain s_m, the ideal uniaxial tensile strength σ_t along the [111] direction, and the corresponding deformation extent t_m. It is noteworthy that the ideal tensile strength may exhibit possible dependence on the choice of the exchange-correlation term (E_{xc}) in the Hamiltonian. To probe the effects of this dependence, we calculated σ_t of Al and Ir using PW19 (Ref. 11) and Perdew-Burke-Ernzerhof (PE).[17] The discrepancy in the total energy per atom for these two E_{xc} terms amounts to 1 eV/6 for Al and 3.5 eV/6 in the case of Ir. As testified by our computations using PW19 (see Table II) and PE, which yield σ_t=10.79 and 49.7 GPa for Al and Ir, respectively, the variations in the ideal tensile strength due to the choice of E_{xc} are negligible. Consequently, we shall restrain our analysis to the calculations performed with PW19. As for the Cauchy pressure, the results are plotted in Figs. 5–7.

In order to probe the relationship between the electronic structure and ductility features of fcc metals, the electron localization function (ELF) is exploited. It is worth mentioning that ELF is more suitable than the electronic charge density in describing chemical bonds since it amplifies the bonding features of a given electron distribution and permits comparison of the bonding of different electron distributions on an absolute scale.[18] The explicit formula of ELF is given by[18,19]

$$\mathrm{ELF} = \frac{1}{1 + \left(\frac{D(\vec{r})}{D_h(\vec{r})}\right)^2}, \tag{6}$$

with

$$D(\vec{r}) = \frac{1}{2}\nabla_{\vec{r}}\nabla_{\vec{r}'}\rho(\vec{r},\vec{r}')|_{\vec{r}=\vec{r}'} - \frac{1}{8}\frac{|\nabla n(\vec{r})|^2}{n(\vec{r})}, \tag{7}$$

and

$$D_h(\vec{r}) = \tfrac{3}{10}(3\pi^2)^{2/3} n(\vec{r})^{5/3}, \tag{8}$$

where ρ is the first-order reduced (spin-integrated) density matrix. $D(\vec{r})$ is the von Weizsäcker kinetic-energy functional and $D_h(\vec{r})$ is the kinetic-energy density of a uniform electron gas with a spin density equal to the local value of $n(\vec{r})$. In the case of extreme delocalization, ELF assumes values close to zero while in the case of high localization, it is close to one. In the regions where the valence charge distribution is similar to the homogeneous electron gas, the ELF comes to 0.5. ELF is implemented in the VASP. The calculations were performed using the orthorhombic fcc unit cell described above with periodic boundary conditions at equilibrium and under shear. The ELF contour plots of Al, Ir, and Pd projected on the $(1\bar{1}0)$ are displayed in Figs. 2–4, respectively.

III. DISCUSSIONS

As demonstrated in Fig. 1, there is a linear correlation between the ratio $\sigma_s/G_{\{111\}}$ and s_m with a slope approximately equal to $\pi/2$, which is consistent with the modified Frankel's model.[20] Additionally, one notices that Al sustains the largest range of deformation among all the scrutinized

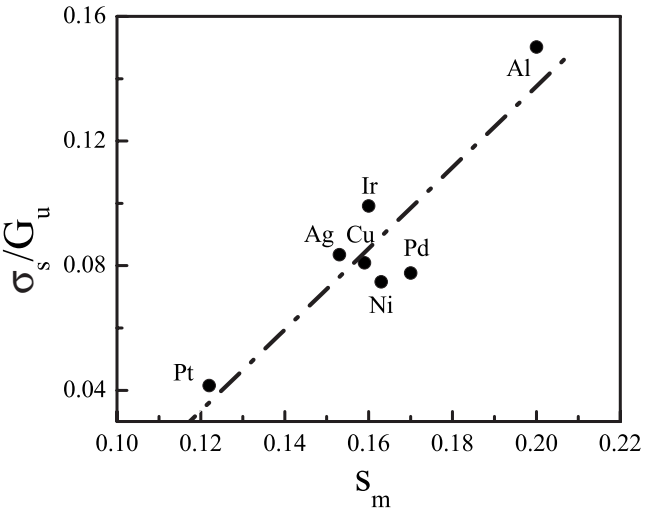

FIG. 1. The ratio of the ideal shear strength over the shear modulus against the shearability s_m.

fcc metals including Ir. The long range of shear deformation (s_m) in Al has lately been identified as a consequence of bond directionality[4] and it has recently been suggested that in general angularly bonded and covalent crystalline structures tend to withstand significant distortion extents, whereas materials with spherically symmetric charge distributions such as copper fail before substantial amount of strain is applied. However, our calculations for the directionally bonded Ir yield a maximal shear strain close to the shearability of Cu. Moreover, Pd [see Fig. 4(a)], whose charge distribution at equilibrium does not exhibit any angular features, is found suffering from longer range of shear distortion compared to Ag, Cu, Ni, Pt, and even Ir. These observations signify the possibility that the range of deformation withstood by an fcc metal does not solely depend on the geometric characteristics of the chemical bonding at equilibrium but other factors such as the bond strength may play some role. In order to rationalize these phenomena, we shall examine the ELF contour plots of Al, Ir, and Pd.

As can be seen in Fig. 2(a), at equilibrium, the valence electrons of Al are either mostly localized in the form of a broad crescent at the immediate neighborhood of the ions and along the orientation normal to the bond path, or they exhibit a small rodlike shape between the non-nuclear attractors (NNAs) separating the adjacent nuclei and in either case, high covalence is detected since the ELF assumes values close to 0.7 in those regions. These angular and covalent features reflect the *s*-*p* hybridization of Al electrons[4] and point to the fact that, under shear deformation, the breaking and reformation of the directional bonds should occur in predominance.[4] When the crystalline structure is deformed, as evinced in Figs. 2(b)–2(d), the electrons in the interstitial regions are transferred toward the NNAs such that a charge depletion process steadily takes place in the aforesaid areas and provokes a marked shrinkage of electron concentration in the interionic space. Thus, the geometric characteristics of the bonding gradually fade away until the material fails. In contrast to Al, copper's valence electrons, whose distribution is rather symmetric in the interionic regions and completely

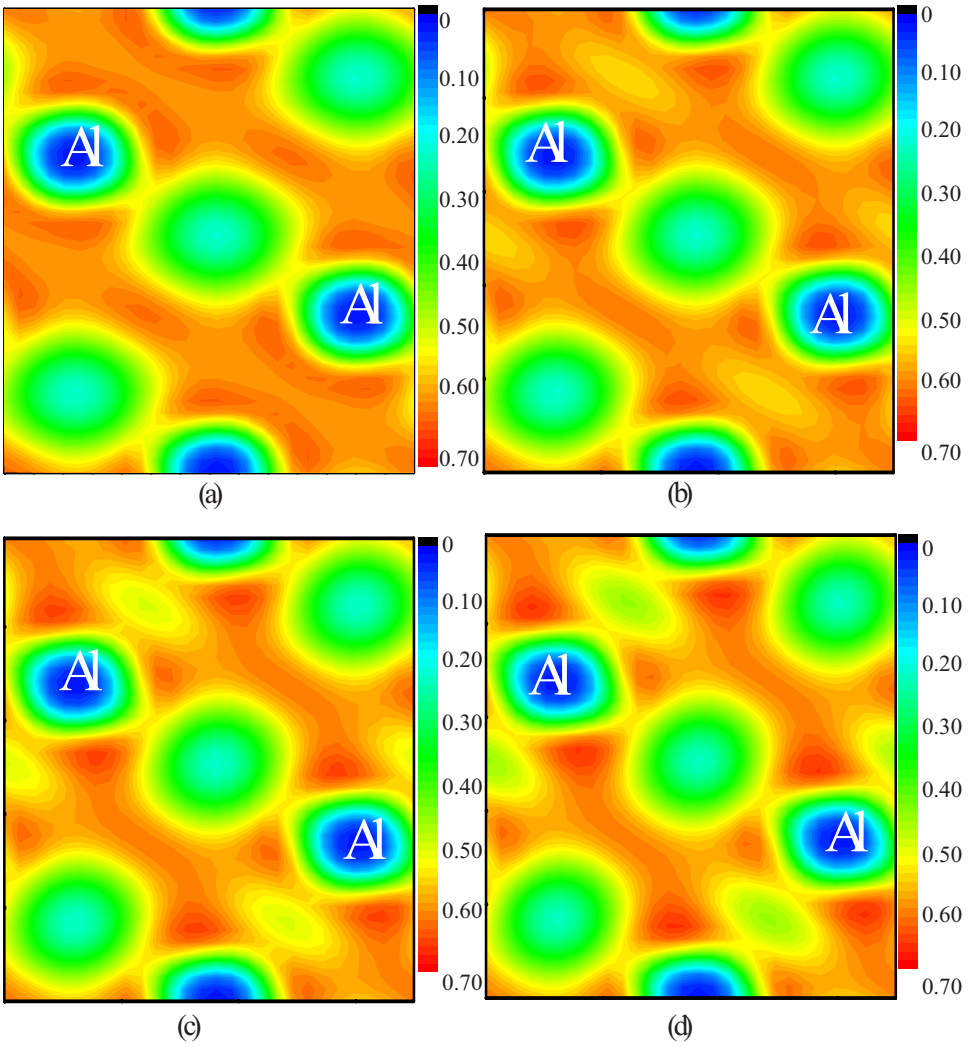

FIG. 2. (Color online) ELF contour plot for Al projected on the $(1\bar{1}0)$ plane for (a) $\gamma=0$, (b) $\gamma=0.5$, (c) $\gamma=0.10$, and (d) $\gamma=0.15$.

deficient in NNAs,[21] are not shifted away from the bonding region and can easily reform the broken bonds due to the lack of geometric constraints until the applied strain is high enough to halt the process. Thus, compared to Al, copper requires smaller strain.[4,20] The current ELF calculations confirm this explanation on the discrepancy between the ideal strain scopes of Al and Cu.

In the case of Ir, at equilibrium, the immediate neighborhood of the Ir nuclei does not enclose a significant portion of the charge carriers' population, as the valence electrons are principally detected in the narrow interstitial regions separating the ions and the NNAs [see Fig. 3(a)]. This geometric feature of iridium's electron distribution, which contrasts it with the other fcc transition metals scrutinized in the present work, stems from the restrictions dictated by the *d*-band filling[22] and has resulted in the formation of thick rodlike bonds. When subjected to shear distortion, the Ir chemical bonding resists the deformation before suffering a bond breaking process as the electrons are transferred away from the bond path toward the numerous NNAs with the applied strain nearing the shearability of the crystal. Subsequently, the chemical bonding is irreversibly broken. It is noteworthy that, during this whole process, the value of ELF never exceeds 0.5, which implies that the bonding of Ir, like most other metals, is only partially covalent at the equilibrium state as described by Silvi and Gatti,[21] and that it remains so even when sheared. This observation provides further evidence in support of the rationalization formulated in terms of bond strength and proposed by the authors in Ref. 22. Thus, when sustaining shear distortion, the strong bonds of Ir, enjoying greater exchange energy compared to other fcc metals,[22] vigorously counterbalance the charge depletion process until few electrons are left along the bond path to compensate the effects induced by the bond breaking and ultimately, the ions can no longer be held together. Consequently, a large stress is required to shear Ir monocrystals, hence its abnormally high shear modulus and its peculiarly significant shear and tensile strengths. Moreover, the one way traffic of electrons toward the NNAs from the valence attractors provoked by the irregular geometric features of iridium's electron distribution further enhances the brittle failure of the solid, thus accounting for the rather small deformation extent of Ir compared to Al.

As for Pd, whose valence charge distribution is broadly spherical although inhomogeneous around the ions due to the presence of the NNAs of rectangular shape [see Fig. 4(a)], the electron concentration along the bond path and in the bulk of interstitial region exhibits a gluelike character except

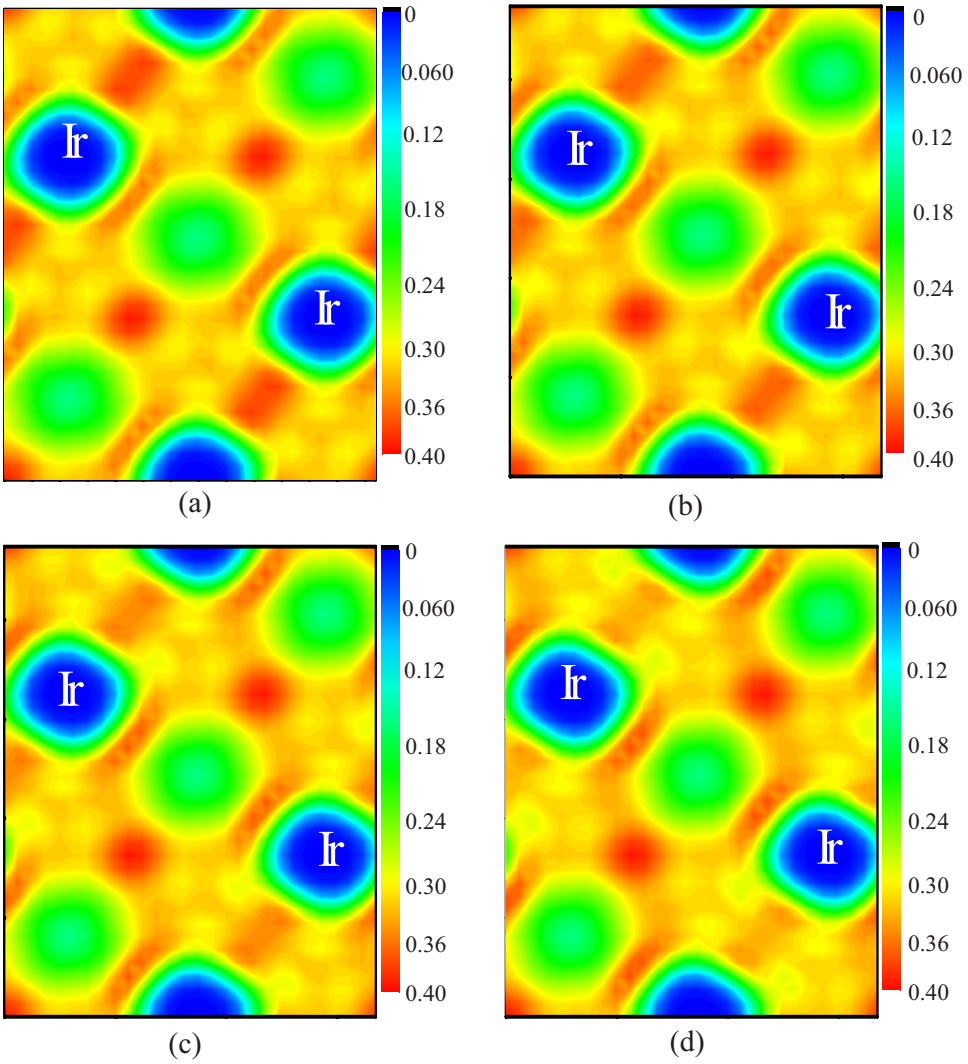

FIG. 3. (Color online) ELF contour plot for Ir projected on the $(1\bar{1}0)$ plane for (a) $\gamma=0$, (b) $\gamma=0.4$, (c) $\gamma=0.8$, and (d) $\gamma=0.12$.

for small triangular electron pockets of comparatively high localization in the interionic space as shown in Figs. 4(a) and 4(b). Thus, the chemical bonding of the ions essentially results from the gluelike network generated by the valence electrons. However, the meager directionality of Pd bonds coupled with its low bond strength[22] seems to confer to Pd peculiar geometric constraints capable of hindering the bond breaking process since the charge depletion in the interionic areas effectively occurs only after 12% of deformation [see Fig. 4(d)]. Consequently, this allows the crystalline structure to experience an extended shear distortion range surpassed only by aluminum. This corroborates the general notion that angular features in the bonding increase the distortion scope of solids.[20] Nevertheless, unlike Al and Ir, the aforesaid directional characteristics in Pd tend to be rather very sparse.

In this study, we have also examined the ELF contour plots of Ag, Pt, and Ni. Silver and platinum both dispose of more or less inhomogeneous spherical charge distributions around the ions. However, unlike Pt, which has NNAs, Ag electron distribution is short of any NNAs but it rather exhibits broad rectangular regions along the bond path and small spotlike areas in the interstice with low electron localization (ELF$\approx$0.14–0.17) compared to the bulk of the interionic space where ELF usually reaches values between 0.175–0.21. These zones with weak electron localization are widened only after the applied strain nears $0.73s_m$ and they gradually spread almost all over the interatomic space. In the case of nickel, whose valence electrons roughly create wide triangles close to the ions, it endures a bond breaking process during which the valence electrons spread away from the nuclei neighborhood toward the interionic interstice. In the case of all these three metals, the ELF always remains below 0.5. It is of note that our calculations seem to imply that the NNAs do not play a primary role in the nonlinear response of fcc metals. In the light of these observations on the electronic properties of fcc metals, we shall now assess the various performance indicators employed to discriminate ductile crystals from brittle ones.

Among the most widely used malleability measures figure the G/B ratio and the Cauchy pressure $(C_{12}$-$C_{44})$. The ratio of shear and bulk moduli distinguishes the fcc ductile metals by assigning values larger than 0.5 to brittle ones. Recently, this criterion has also been verified for intermetallic fcc compounds through first-principles calculations.[14,23] As regards the Cauchy pressure, it is often evoked to explore the geometry of the chemical bonding since it yields negative values for directionally bonded solids such as Si, and positive ones for ductile metals exemplified by Ni and Al. The aforemen-

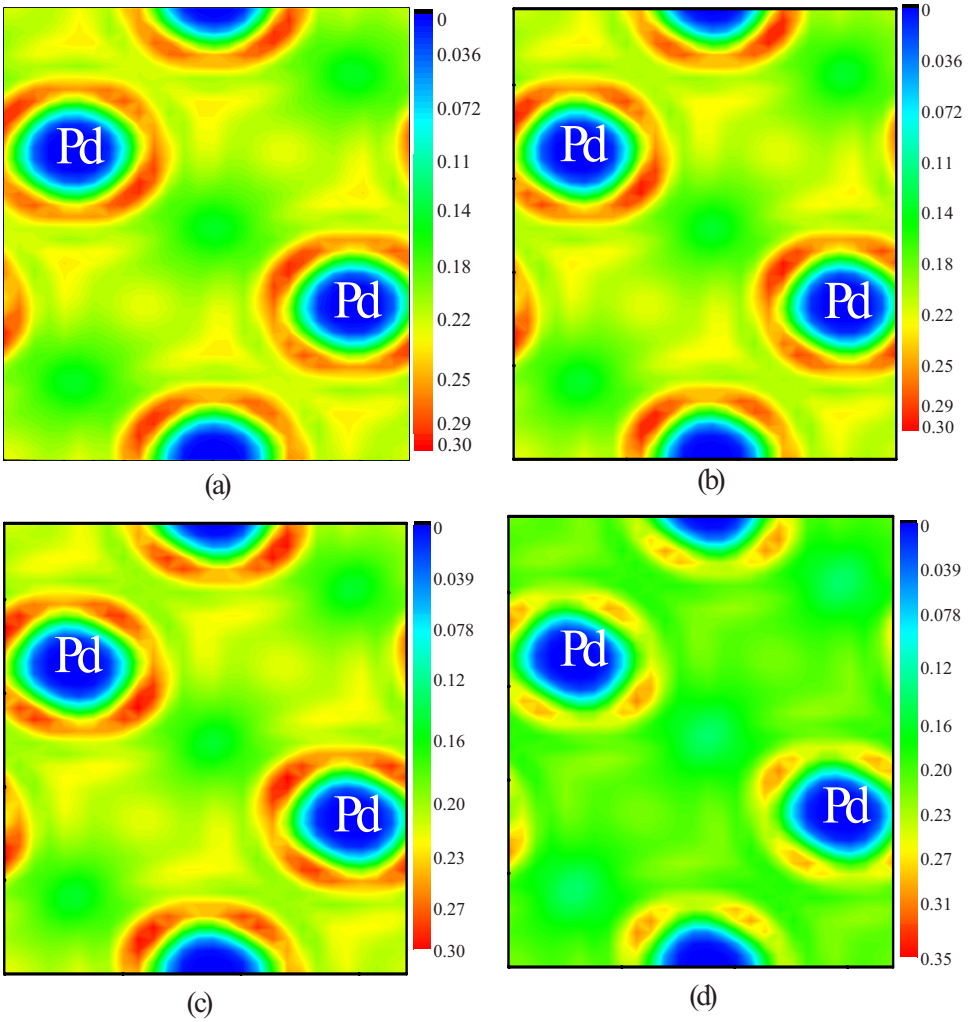

FIG. 4. (Color online) ELF contour plot for Pd projected on the (111) plane for (a) $\gamma=0$, (b) $\gamma=0.4$, (c) $\gamma=0.8$, and (d) $\gamma=0.12$.

tioned ductility gauges are plotted against each other in Fig. 5. As can be seen, there is some divergence between these two indicators, when one closely examines the case of Ag, Cu, Ni, and Al. In the case of Cauchy pressure, Ag, Cu, and Ni evince nearly the same values while the angularly bonded Al has a slightly smaller value. Moreover, C' for Pd and Pt is comparatively large and it takes a negative value for Ir. This trend follows the general behavior of C' as expressed above and fails to clearly single out fcc metallic structures with directional bonding when compared with our results from ELF calculations. As for the G/B ratio, the calculated results present a rather broad decreasing trend from the most ductile fcc metal to the most brittle one. Nevertheless, certain degeneracy is noted as G/B gives similar values for Al and Ag, and groups Cu and Ni together. Consequently, the G/B ratio can only be viewed as a broad indicator of malleability, which does not necessarily reflect the angular characteristics of the valence electrons. Given the significant role of the geometric features of the bonds in shaping the behavior of solids under distortion, the current discussion of the two most commonly exploited ductility indicators reveals the necessity of elaborating a new criterion capable of magnifying these effects in a more lucid fashion.

To evaluate the possibility of developing a better indicator of brittleness, in Fig. 6, both the G/B ratio and the Cauchy pressure are plotted against σ_s/σ_t, the ratio of the ideal shear strength σ_s over the ideal tensile strength σ_t on the (111) plane, for a selection of fcc metals. As can be observed in Fig. 6(b), G/B and σ_s/σ_t follow the same broad linear trend for most metals with the exception of Al. They both show low values for ductile crystals and high values for brittle iridium. However, the σ_s/σ_t ratio for Al assumes a larger value compared to the G/B ratio for this same metal, and sets it completely apart from Cu, Ag, and Ni. This conspicuous difference between the respective values of G/B and σ_s/σ_t for Al infers that, in contrast to G/B, σ_s/σ_t may convey the disparity between the bonding geometries of the fcc metals in a more clear-cut fashion. While this noteworthy divergence on Al might be attributed to the fact that G/B is a somewhat simplified form of σ_s/σ_t,[2] it also implies that not only does the σ_s/σ_t ratio distinguish brittle fcc solids in an equally accurate manner but, in addition, it is susceptible of revealing the directional characteristics of the bonding, which partly dictate the performance of the crystalline structure and their extent of deformation under nonlinear distortion. It is worth mentioning that, without a systematic evaluation of σ_s/σ_t for different types of ductile and brittle materials, the determination of the exact numerical criterion for assessing the malleability based on σ_s/σ_t is not possible but as shown in the plot, it is comprised within the range of

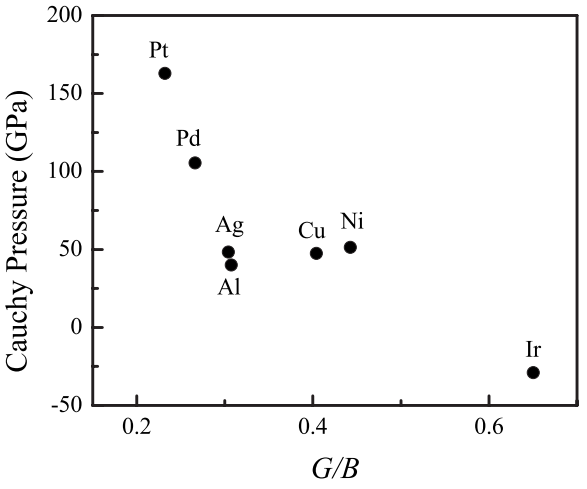

FIG. 5. The ratio G/B against the Cauchy pressure C_{12}-C_{44}.

0.36–0.40 (see Fig. 6, the region separating ductile Al from brittle Ir), which obviously falls behind the critical value of 0.5 for G/B.

As can be observed from Fig. 6(a), there is a stronger linear correlation between Cauchy pressure and σ_s/σ_t. Given that the Cauchy pressure is a macroscopic measure of bond directionality,[3,22] it can be concluded that the ratio σ_s/σ_t provides pieces of information regarding the angular features of the chemical bonding. This further supports the surmise put forth in the previous section and hinting at the advantage of σ_s/σ_t over the widely used G/B ratio in appraising the response of directionally bonded crystals under long-range distortion. While the values of Cauchy pressure and σ_s/σ_t for Al differ by a noticeable amount, in both cases, there is a similar trend that sees Al following Cu and Ag, both having spherically symmetric valence charge distributions, and preceding Ir that disposes of strong angular bonds. This is suggestive of the fact that in the specific case of fcc metallic structures, C' falls short of contrasting the specific divergences between different metals in a significant manner. Consequently, the ratio σ_s/σ_t can be said to offer a more detailed depiction of the competition between the plastic shear and fracture stress, and their relationship to the angular characteristics of the valence electron distribution of fcc metals.

With the aim of investigating potential relationship of s_m/s_t, the ratio of shearability (s_m) over tensibility (s_t), to Cauchy pressure (G/B and σ_s/σ_t), the ratio of the ideal strains is plotted against the above mentioned malleability measures as illustrated in Fig. 7. In general, a linear correlation ranging from the ductile Pt to the brittle Ir is observed; nonetheless, it appears that the ratio s_m/t_m, unlike the ratio of the ideal shear over tensile strengths, fails to draw an unambiguous distinction between Al and other ductile metals since the value of this ratio for Al falls within the same range as other well-known fcc metals exemplified by silver among others. A significant divergence between the Cauchy pressure and the ratio of ideal strains can also be noticed, as there is a situation of degeneracy with the values of Cauchy pressure for Ni, Cu, and Ag that is removed by the ratio s_m/t_m. In the case of Pd, the s_m/t_m ratio for this solid is of the same order

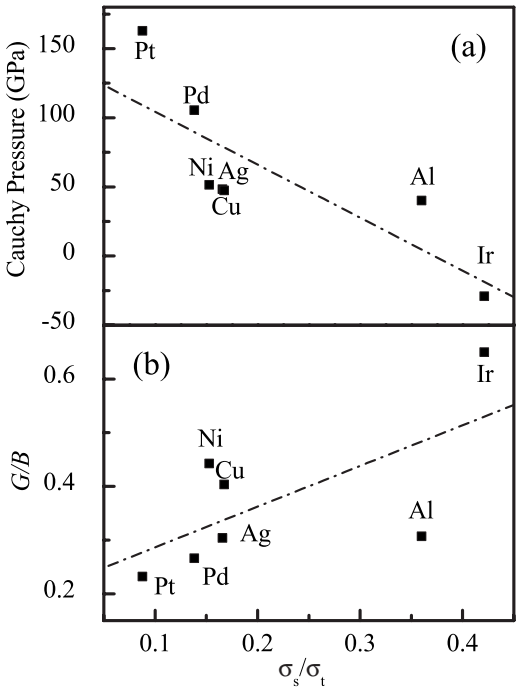

FIG. 6. (a) The ratio G/B and (b) the Cauchy pressure against the ratio of the ideal shear and tensile strengths.

of magnitude as those for other well known ductile fcc metals, and more precisely it falls between Ni and Cu. On the contrary, the Cauchy pressure value for Pd sets it apart from Ni, Cu, and Ag, thus possibly hinting at geometric features brought about by the scanty electron pockets in interstitial area as portrayed by Figs. 4(a)–4(d).

As evinced in Fig. 7, there is a notable difference between σ_s/σ_t and s_m/s_t, as far as Ni, Cu, and Ag are concerned. Here again, the ratio of the ideal strains simply resolves the degeneracy of the values of σ_s/σ_t for these more or less equally ductile crystals; whereas the ratio of the ideal strengths presents the advantage of sieving the directionally bonded crystalline structures from those with symmetric charge distributions as discussed previously. As pertaining to the relationship of G/B to s_m/s_t, Fig. 7(c) testifies the lack of any strong linear correlation between G/B and s_m/t_m, even though the general trend followed by these two parameters is somewhat similar. In particular, Pd has a very small value for G/B while its ratio of the ideal strains assumes a considerably larger one. Yet, this divergence can hardly be attributed to any atomic-scale features. It is noteworthy that, despite the fact that the value of s_m/t_m for Al is not particularly outstanding, it is higher than that of the well-known ductile fcc metals, thus suggesting that the ratio s_m/t_m may have an advantage over the macroscopic indicators in this regard. Combining these observations with the discussions on the previous performance indicators, one can conclude that the ratio of the ideal strengths is probably a better measure of ductility/brittleness.

IV. CONCLUSIONS

Through systematic *ab initio* density-functional theory-based calculations, the ratio of ideal shear strength over ten-

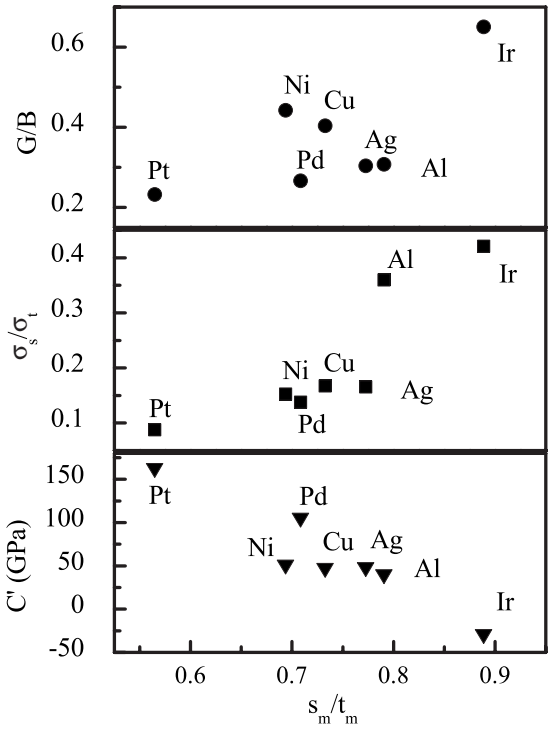

FIG. 7. The Cauchy pressure, the ratio of the ideal strengths, and the ratio G/B against the ratio of shearability over tensibility.

sile strength and the electron localization function for a broad selection of fcc metals are evaluated with the purpose of elucidating the electronic factors underlining their behavior under nonlinear distortion, and in order to establish a more nuanced performance indicator. Although Al is found to sustain the longest range of deformation due to its angular and moderately covalent bonds, the study of the specific case of Ir, which disposes of large ideal strengths but a shearability similar to Ni and Cu, shows that the angular characteristics of the chemical bonding do not constitute the unique factor controlling the shear distortion scope of fcc crystals since the strength of the solids may also play an essential role. As pertaining to Pd, the computations presented in the current work suggest that the valence electron distribution of this metal permits the material to withstand a noticeable extent of distortion due to the few electron pockets in the interionic region, which confer geometric constraints to the solid. In addition, the ratio of the ideal strengths σ_s/σ_t is found to be a more potent means of distinguishing ductile metallic solids, as it not only discriminates malleable structures from brittle ones but it also discerns directionally bonded fcc metals. However, it remains to be seen whether this indicator or a similar one can be developed for the bcc metals, a substantial number of which are of interest to materials science.

ACKNOWLEDGMENTS

This research is funded by the Structures and Materials Performance Laboratory (SMPL) of the Institute for Aerospace Research, National Research Council of Canada (NRC), and also by the Natural Sciences and Engineering Research Council of Canada (NSERC).

*Corresponding author; Present Address: Structures and Materials Performance Laboratory, Institute for Aerospace Research, National Research Council of Canada, Montreal Road M-17 Ottawa, Ontario, Canada K1A 0R6; FAX: 1-613-949-8165; kuiying.chen@nrc-cnrc.gc.ca

[1] J. R. Rice, J. Mech. Phys. Solids **40**, 239 (1992).
[2] S. F. Pugh, Philos. Mag. **45**, 823 (1953).
[3] R. A. Johnson, Phys. Rev. B **37**, 3924 (1988).
[4] S. Ogata, Ju Li, and S. Yip, Science **298**, 807 (2002).
[5] J. Frenkel, Z. Phys. **37**, 572 (1926).
[6] D. Roundy, C. R. Krenn, M. L. Cohen, and J. W. Morris, Philos. Mag. A **81**, 1725 (2001).
[7] D. M. Clatterbuck, D. C. Chrzan, and J. W. Morris, Philos. Mag. Lett. **82**, 141 (2002).
[8] D. Roundy, C. R. Krenn, M. L. Cohen, and J. W. Morris, Phys. Rev. Lett. **82**, 2713 (1999).
[9] G. Kresse and J. Furthmuller, Comput. Mater. Sci. **6**, 15 (1996).
[10] G. Kresse and J. Furthmuller, Phys. Rev. B **54**, 11169 (1996).
[11] J. P. Perdew, J. A. Chevary, S. H. Vosko, K. A. Jackson, M. R. Pederson, D. J. Singh, and C. Fiolhais, Phys. Rev. B **46**, 6671 (1992).
[12] P. E. Blöchl, Phys. Rev. B **50**, 17953 (1994).
[13] G. Kresse and D. Joubert, Phys. Rev. B **59**, 1758 (1999).
[14] K. Chen, L. R. Zhao, and J. S. Tse, J. Appl. Phys. **93**, 2414 (2003).
[15] G. Simmons and H. Wang, *Single Crystal Elastic Constants and Calculated Aggregate Properties: a Handbook*, 2nd ed. (M.I.T. Press, Cambridge, Massachusetts, 1971).
[16] A. T. Paxton, P. Gumbsch, and M. Methfessel, Philos. Mag. Lett. **63**, 267 (1991).
[17] J. P. Perdew, K. Burke, and M. Ernzerhof, Phys. Rev. Lett. **77**(18), 3865 (1996).
[18] L. De Santis and R. Resta, Surf. Sci. **450**, 126 (2000).
[19] A. D. Becke and K. E. Edgecombe, J. Chem. Phys. **92**, 5397 (1990).
[20] S. Ogata, Ju Li, N. Hirosaki, Y. Shibutani, and S. Yip, Phys. Rev. B **70**, 104104 (2004).
[21] B. Silvi and C. Gatti, J. Phys. Chem. A **104**, 947 (2000).
[22] S. Kamran, K. Chen, L. Chen, and L. Zhao, J. Phys.: Condens. Matter **20**, 085221 (2008).
[23] K. Chen, L. Zhao, and J. S. Tse, Phys. Lett. A **331**, 400 (2004).